Optimization of operational variables and kinetic modeling for photocatalytic removal of Direct Blue 14 from aqueous media by ZnS nanoparticles

Ali Mehrizad and Parvin Gharbani

ABSTRACT

Zinc sulfide nanoparticles (ZnS-NPs) were synthesized via a simple and facile co-precipitation method and were characterized by X-ray diffraction (XRD), field emission scanning electron microscopy (FE-SEM) and diffuse reflectance spectroscopy (DRS). Photocatalytic activity of synthesized nanoparticles was evaluated in removal of double azo dye Direct Blue 14 (DB14) from aqueous media. Optimization of photocatalytic removal of DB14 was studied using response surface methodology (RSM). Based on the results, DB14 removal efficiency increased with increasing intensity and duration of UV light irradiation, whereas the higher pH and higher initial dye concentration were unfavorable. Under optimum conditions (initial DB14 concentration $=10$ mg L^{-1}, ZnS-NPs amount $= 0.7$ g L^{-1}, pH $= 3.5$, UV light intensity $=16$ W m^{-2}, and irradiation time $= 48$ min), dye removal efficiency reached up to 88.26%. In continuation of our researches, non-linear regression analysis was used to development a kinetics model based on the Langmuir–Hinshelwood model and an empirical equation was obtained for estimation of apparent pseudo-first-order rate constant (k_{ap}) as a function of the operational variables. Findings indicated a high similarity was between the model prediction and experimental results.

Key words | Direct Blue 14, kinetic modeling, photocatalysis, response surface methodology, ZnS nanoparticles

Ali Mehrizad (corresponding author)
Department of Chemistry, Tabriz Branch,
Islamic Azad University,
Tabriz,
Iran
E-mail: *mehrizad@iaut.ac.ir*

Parvin Gharbani
Department of Chemistry, Ahar Branch,
Islamic Azad University,
Ahar,
Iran

INTRODUCTION

Water pollutants often contain organic and inorganic chemical compounds that have undesirable effects on human health and other organisms. Dye is one of the most important chemicals which influences the esthetic merit of water and prevents the penetration of sunlight required for photosynthesis to occur in aquatic environments. In addition, such compounds cause mortality in the aquatic ecosystem due to their toxicity (Agarwal *et al.* 2016; Asfaram *et al.* 2016). Synthetic dyes are used in many fields such as the textile, paint, paper, leather, and food industries. It is obvious that creating colored effluents in these industries is unavoidable and, as such, there should be a remedy before the discharge of such effluents to the environment (Padmanaban *et al.* 2016). Direct Blue 14 (DB14), which was taken as the model compound in the current study, is a double azo dye and can be found in the aforementioned industrial effluents. As is known, azo dyes are recalcitrant and persistent towards breakdown and because of their high degree of persistence in the environment, they can cause irreparable damage to flora and fauna (Punzi *et al.* 2015; Zhang *et al.* 2016). According to the literature review, the use of simple and efficient approaches is crucial, since numerous attempts have been made to destroy such contaminants (Barragan *et al.* 2007; Wang *et al.* 2012; Kong *et al.* 2016; Lalnunhlimi & Krishnaswamy 2016). It is clear that advanced oxidation

doi: 10.2166/wh.2017.269

processes (AOPs) have benevolent properties in the field of environmental remediation and the ample verification of this application in wastewaters' treatment (Saien *et al.* 2011; Antonin *et al.* 2015; Lelario *et al.* 2016). Photocatalytic processes are the most popular AOPs performed using a semiconductor and the presence of a suitable radiation source. Various semiconductors are in vogue for this objective and due to the non-toxic nature and high negative reduction potential of excited electrons in zinc sulfide (ZnS), because of its higher conduction band position in aqueous media, ZnS is an appropriate alternative for this purpose. In addition, this material displays fine photocatalytic activity due to trapped holes arising from surface defects on the sulfides (Sakkas *et al.* 2010; Di Paola *et al.* 2012; Kaur *et al.* 2015; Yin *et al.* 2016). One of the most important aspects in the field of heterogeneous photocatalysis processes is the kinetics studies based on regression analysis (Yatmaz *et al.* 2004; Sheidaei & Behnajady 2015). Behnajady & Modirshahla (2006) developed a kinetics model based on the nonlinear regression analysis for the photocatalytic decolorization of an azo dye in aqueous TiO_2 slurry. Their results revealed that the kinetics of decolorization of dye in the UV/TiO_2 process fit well by pseudo-first-order kinetics. In another survey, a pseudo-first-order model was observed for the photoreduction of Cr(VI) by immobilized ZnO at different operational conditions (Behnajady *et al.* 2012).

In the current research, a simple co-precipitation method was used to synthesize ZnS nanoparticles (ZnS-NPs). The experimental design was carried out using response surface methodology (RSM) conducted to remove DB14 azo dye by synthesized nanoparticles. Finally, kinetics modeling of the process was performed.

EXPERIMENTAL

Materials

Zinc acetate dihydrate ($Zn(CH_3COO)_2.2H_2O$) and sodium sulfide flakes (Na_2S) were purchased from Merck (Germany) and Loba Chemie (India), respectively. DB14 was supplied by Acros Organics (USA), and its characteristics are illustrated in Table 1. In all procedures, double distilled water was used.

Preparation and characterization of ZnS-NPs

The synthesis of ZnS-NPs by co-precipitation method often requires a capping agent (such as mercaptoethanol) and high operation temperature (Chandrakar *et al.* 2015). In this study, ZnS-NPs were synthesized by a simplified method (at room temperature) which did not require a capping agent. An aqueous solution of Na_2S (100 mL, 0.5 M) was magnetically stirred in a three-neck round-bottom flask under the presence of N_2 gas. After 30 min, a solution of zinc acetate (100 mL, 0.5 M) was added to the stirred solution of Na_2S, drop-wise. The reaction was allowed to proceed under vigorous stirring for 1 h at room temperature. Afterwards, the milky white color precipitate was collected by centrifugation and repeatedly rinsed with ethanol and

Table 1 | Characteristics of DB14

Chemical structure	Molecular formula	Molecular weight (g mol^{-1})	λ_{max} (nm)
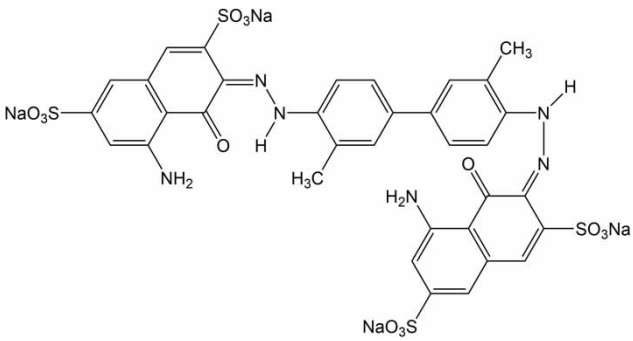	$C_{34}H_{24}N_6O_{14}S_4Na_4$	960.81	665

deionized water in order to remove impurities. Finally, it was left to dry for 48 h at room temperature and thereafter crushed to obtain a fine powder. The prepared ZnS-NPs were characterized in detail by X-ray diffraction (XRD, X'Pert Pro, Panalytical) and field emission scanning electron microscopy (FE-SEM, SIGMA, Zeiss) equipped with energy dispersive X-ray (EDX, Oxford Instruments). The diffuse reflectance spectroscopy (DRS) spectrum was obtained using a UV-2550 Shimadzu spectrophotometer.

Design of experiments

Nowadays, the use of experimental designs to find ideal process settings and achieve optimal performance is becoming inevitable. Several professional softwares have been developed for this purpose, of which, the Design-Expert (DX) software provides a highly efficient design of experiments for RSM. Accordingly, this study utilized the DX7 software for the design of experiments by RSM-based central composite design (CCD). Five operational variables, viz. initial DB14 concentration, ZnS-NPs amount, pH, intensity and duration of UV light irradiation were selected and studied at five levels ($-\alpha$, -1, 0, $+1$, $+\alpha$). Values of α can be calculated by $\alpha = 2^{k/4}$, where k is the factor number. Table 2 lists the ranges and levels of the operational variables.

Based on the DX7 software offered, a total of 32 experiments were conducted and the results analyzed. The relationship between the input variables and outcome variable can be explained by the following mathematical model:

$$y = \beta_0 + \sum_{i=1}^{k} \beta_i x_i + \sum_{i=1}^{k} \beta_{ii} x_i^2 + \sum_{i=1}^{k} \sum_{j=1}^{k} \beta_{ij} x_i x_j + \varepsilon \quad (1)$$

Table 2 | Ranges and levels of the operational variables

	Range and level				
Variable	$-\alpha$	-1	0	$+1$	$+\alpha$
$[DB14]_0$ (mg L^{-1})	5	10	15	20	25
$[ZnS\text{-}NPs]_0$ (g L^{-1})	0.2	0.4	0.6	0.8	1
pH	1.5	3.5	5.5	7.5	9.5
I_0 (W m^{-2})	4	8	12	16	20
Time (min)	12	24	36	48	60

where y is the anticipated response and k is the number of autonomous variables. x_i and x_j are coded autonomous variables. x_i^2 and $x_i x_j$ represent the quadratic and interaction effects of autonomous variables, respectively. β_0 is the constant. β_i, β_{ii}, and β_{ij} are coefficients for main, quadratic, and interaction effects, respectively. ε is the residual associated with the experiments (Sakkas *et al.* 2010).

Photocatalysis experiments

Batch experiments were undertaken in a cylindrical glass reactor on a magnetic stirrer (300 rpm) by agitation of the desired amounts of ZnS-NPs in 100 mL of DB14 solution at a given pH. UV-C irradiation was performed by a 30 W mercury lamp (Germicidal, China), placed at the top of the reactor in a wooden cabin, and the intensity of UV light was measured by a Lux-UV-IR meter (Leybold, Germany). After a definite time interval, samples were collected and centrifuged. The DB14 solution absorbance was measured by UV-Vis spectrophotometer (UV mini-1240, Shimadzu) at 665 nm. The removal efficiency (%) was computed by Equation (2):

$$R\,(\%) = \left(\frac{C_0 - C_t}{C_0}\right) \times 100 \quad (2)$$

where C_0 and C_t are the concentration of dye (mg L^{-1}) when the reaction time is 0 and t, respectively.

It is to be noted that similar experiments were done in the dark for evaluation of dye adsorption. Nevertheless, the dye removal efficiency was negligible.

RESULTS AND DISCUSSION

Characterization of ZnS-NPs

As can be seen from the XRD pattern of as-prepared powder (Figure 1), the appearance of three main dominant peaks at $2\theta = 28.73$, 47.9, and 56.56° indicates the formation of cubic lattice structure of ZnS, which match well with the standard XRD pattern of cubic ZnS reported in the JCPDS Powder Diffraction (Guinier 1963). The FE-SEM image (Figure 2 (a)) proves the morphology of ZnS particles is well formed at nanoscale and the histogram of particle size distribution

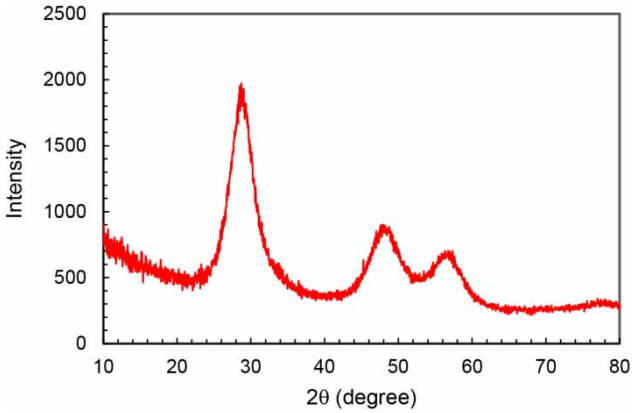

Figure 1 | XRD pattern of synthesized ZnS particles.

shows the particles in the size of a range from 20 to 60 nm with a mean diameter of 41.72 nm (Figure 2(b)). The EDX spectrum (Figure 2(c)) indicates the presence of elemental zinc and sulfur signals, as well. The value of ZnS-NPs band gap was estimated to be 3.64 eV by the UV-DRS spectrum (data not shown here).

Optimization of operational variables by RSM

The operational variables of initial DB14 concentration, ZnS-NPs amount, pH, intensity and duration of UV light irradiation were investigated for evaluation of DB14 removal by UV/ZnS-NPs process. Details of the designed matrix by CCD as well as actual and predicted results are given in Table 3.

To verify the model provided by software, analysis of variance (ANOVA) was conducted (Table 4).

According to the data in Table 4, the model *F*-value of 212.02 implies that the model is significant, and comparison with the actual and predicted results in Table 3 indicates this fact. Also, the Pred *R*-squared value of 0.9632 is in reasonable agreement with the Adj *R*-squared value of 0.9715 and this also confirms the significance of the model. In Table 4, values of Prob $>F$ less than 0.0500 indicate model terms are significant. In this case, initial DB14 concentration, pH, intensity and duration of UV irradiation are significant model terms and a final reduced equation can be obtained as follows:

$$R(\%) = 5.80 - 1.88\,[DB14]_0 - 1.54\,pH + 2.82\,I_0 + 1.18\,Time \quad (3)$$

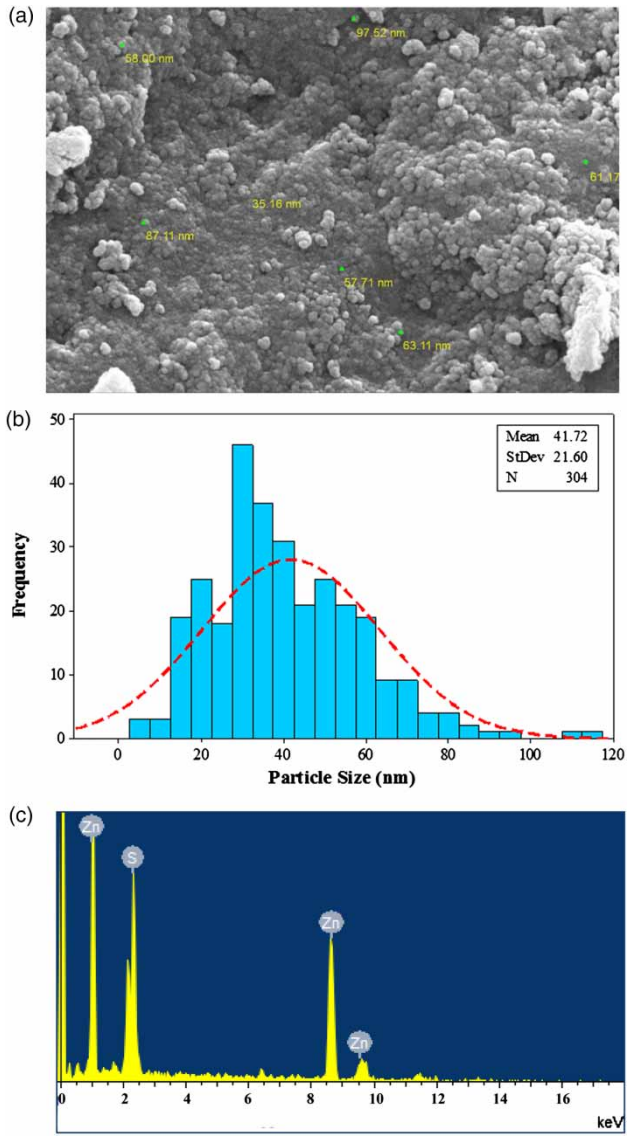

Figure 2 | (a) FE-SEM image; (b) histogram of size distribution; (c) EDX spectrum of ZnS-NPs.

Likewise, statistics curves were plotted to ensure the validity of the model. As depicted in Figure 3, the linear quiddity of the normal plot of residuals and haphazard propagation of the residual versus run number, confirms the adequacy of the suggested model.

Since all the model statistics and diagnostic plots are fine, the experimental designs with drawing of three-dimensional graphs and finding the optimum conditions were followed.

It is clear from Figure 4(a)–4(e) for all levels of ZnS-NPs amount, DB14 removal efficiency increased with increasing

Table 3 | Designed matrix by CCD as well as actual and predicted results

	Operational parameters					R (%)	
Run	$[DB14]_0$ (mg L^{-1})	$[ZnS\text{-}NPs]_0$ (g L^{-1})	pH	I_0 (W m^{-2})	Time (min)	Actual	Predicted
1	20	0.4	7.5	16	24	35.32	29.54
2	15	0.6	9.5	12	36	35.83	36.83
3	20	0.4	7.5	8	48	32.92	35.41
4	20	0.4	3.5	8	24	18.68	13.10
5	20	0.8	7.5	16	48	62.03	57.86
6	15	0.6	1.5	12	36	53.78	51.86
7	15	0.6	5.5	12	36	49.59	45.66
8	20	0.4	3.5	16	48	64.32	64.32
9	5	0.6	5.5	12	36	64.43	64.56
10	15	1	5.5	12	36	44.78	48.49
11	20	0.8	7.5	8	24	12.78	8.19
12	10	0.4	7.5	16	48	80.01	76.94
13	10	0.8	3.5	16	48	83.20	85.45
14	10	0.8	3.5	8	24	34.25	33.28
15	15	0.6	5.5	12	36	42.86	45.66
16	10	0.4	7.5	8	24	25.85	25.80
17	10	0.4	3.5	16	24	54.65	54.63
18	15	0.6	5.5	20	36	67.83	68.30
19	15	0.6	5.5	4	36	20.57	23.03
20	15	0.2	5.5	12	36	41.59	42.22
21	20	0.8	3.5	16	24	35.74	37.02
22	15	0.6	5.5	12	12	14.42	17.16
23	10	0.8	7.5	8	48	58.67	55.29
24	15	0.6	5.5	12	36	42.08	45.66
25	15	0.6	5.5	12	36	41.70	45.66
26	25	0.6	5.5	12	36	21.45	26.77
27	15	0.6	5.5	12	36	46.26	45.66
28	20	0.8	3.5	8	48	44.57	42.89
29	10	0.4	3.5	8	48	60.51	60.50
30	10	0.8	7.5	16	24	50.03	49.72
31	15	0.6	5.5	12	36	44.45	45.66
32	15	0.6	5.5	12	60	75.97	77.17

intensity and duration of UV light irradiation, whereas the alkaline pHs and higher initial dye concentration were unfavorable. Indeed, in the UV/ZnS-NPs photocatalytic process, the generation of conduction band electron-valence band hole pairs ($e^-_{CB} + h^+_{VB}$) and consequently hydroxyl radicals' production increased with increment of intensity and time irradiation and more attacks of hydroxyl radicals led to an ascent in dye removal amount (Ertugay & Nuran Acar 2014). The aforementioned explanations are summarized in the following reactions:

Table 4 | ANOVA results for the DB14 removal by UV/ZnS-NPs process

Source	Sum of squares	Df	Mean square	*F*-value	*p*-value prob >*F*
Model	10,329.80	5	2,065.96	212.02	<0.0001
$[DB14]_0$	2,142.73	1	2,142.73	219.90	<0.0001
$[ZnS\text{-}NPs]_0$	9.87	1	9.87	1.01	0.3235
pH	229.46	1	229.46	23.55	<0.0001
I_0	3,037.38	1	3,037.38	315.41	<0.0001
Time	4,874.36	1	4,874.36	500.23	<0.0001
Residual	253.35	26	9.74		
Lack of Fit	207.96	21	9.90	1.09	0.5107

Pred *R*-squared: 0.9632; Adj *R*-squared: 0.9715.

$$ZnS - NPs + h\nu \rightarrow ZnS - NPs\ (e^-_{CB} + h^+_{VB}) \quad (4)$$

$$h^+_{VB} + H_2O \rightarrow H^+ + {}^\circ OH \quad (5)$$

$$h^+_{VB} + OH^- \rightarrow {}^\circ OH \quad (6)$$

$$e^-_{CB} + O_2 \rightarrow {}^\circ O^-_2 \quad (7)$$

$${}^\circ O^-_2 + H_2O + H^+ \rightarrow H_2O_2 + OH^- \quad (8)$$

$$H_2O_2 + e^-_{CB} \rightarrow {}^\circ OH + OH^- \quad (9)$$

On the other hand, increasing the initial concentration of dye reduces the removal efficiency (Figure 4(a) and 4(e)). Several presumed reasons for this occurrence include: the active sites on the surface of photocatalyst are occupied by the dye molecules and, as such, the production of oxidizing species on the surface is diminished; the generation of intermediate species formed by destruction of dye increased with enhancement of dye concentration; thus, there is the probability of rivalry of the intermediate species with the dye molecules

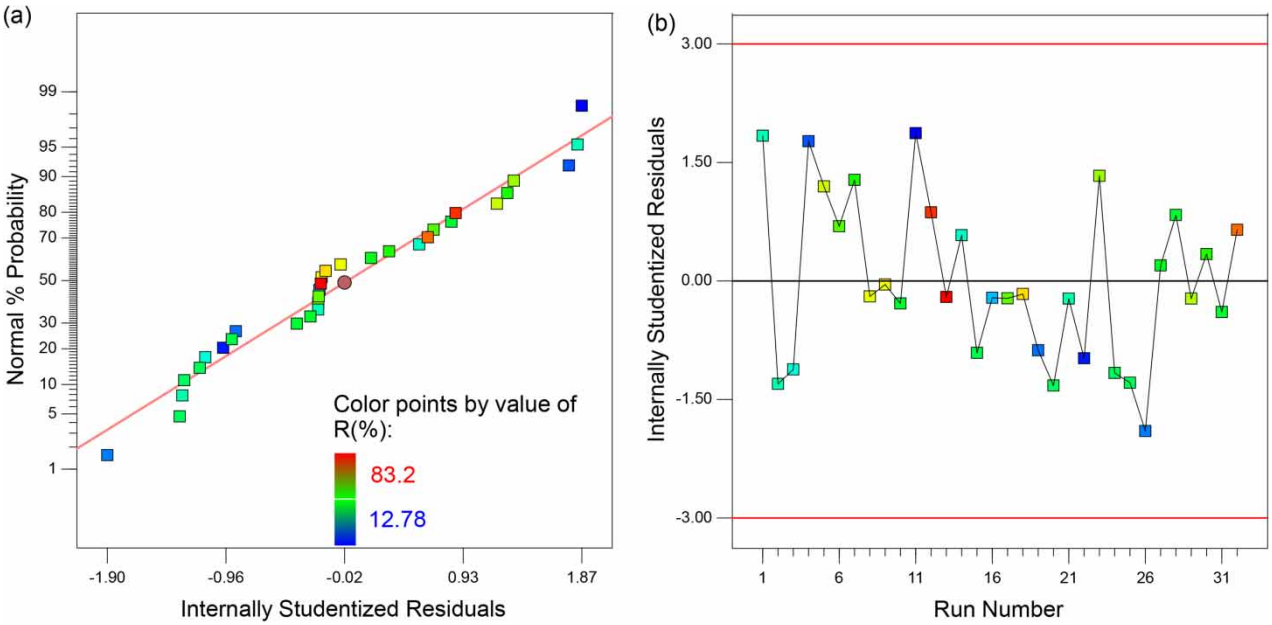

Figure 3 | (a) Normal plot of residuals; (b) residuals vs. run number.

regarding destruction (Hassani *et al.* 2015; Khataee *et al.* 2015).

Figure 4(b) and 4(c) show that the removal efficiency of DB14 dye was improved with reduction of pH. This can be attributed to the fact that since the pH of isoelectric point for ZnS-NPs is about 7 (Pouretedal *et al.* 2009) (i.e., ZnS-NPs surface is positively charged at $pH < 7$ and negatively charged at $pH > 7$), a strong adsorption of the DB14 anionic dye on the ZnS-NPs surface at acidic pHs led to intensification in photodegradation. This result is consistent with the findings of other investigations (Khataee & Zarei 2011).

From the description provided and three-dimensional graphs, it can be concluded that the intensity and the duration of UV light irradiation have a synergetic effect on the DB14 removal amount. Also, a little consumption of catalyst at acidic pHs can accelerate the DB14 removal process by reducing activation energy.

Eventually, optimization of the process by CCD indicated that, under optimum conditions (initial DB14 concentration $= 10\ mg\ L^{-1}$, ZnS-NPs amount $= 0.7\ g\ L^{-1}$, $pH = 3.5$, UV intensity $= 16\ W\ m^{-2}$, and irradiation time $= 48$ min), dye removal efficiency reached 88.26%. This was verified experimentally (90.17%) and is further proof of the success of the designed model.

It is worth noting that similar results were obtained by photolysis process at a longer period of time (>180 min).

Kinetics modeling

According to the literature review, the Langmuir–Hinshelwood kinetics model is the most common model in the study of dye photocatalysis, and is expressed by Equation (10):

$$r = -\frac{dC}{dt} = \frac{kKC}{1 + KC} \tag{10}$$

where r is the reaction rate ($mg\ L^{-1}\ min^{-1}$), k is the reaction rate constant ($mg\ L^{-1}\ min^{-1}$), K is the adsorption constant ($L\ mg^{-1}$), and C is the dye concentration ($mg\ L^{-1}$).

From the viewpoint of some researchers, the competitive adsorption by intermediates must also be considered and so, Equation (10) can be written as follows:

$$r = -\frac{dC}{dt} = \frac{kKC}{1 + KC + \sum K_i C_i} \tag{11}$$

where K_i and C_i are the adsorption equilibrium constant and intermediates concentration, respectively. Based on the

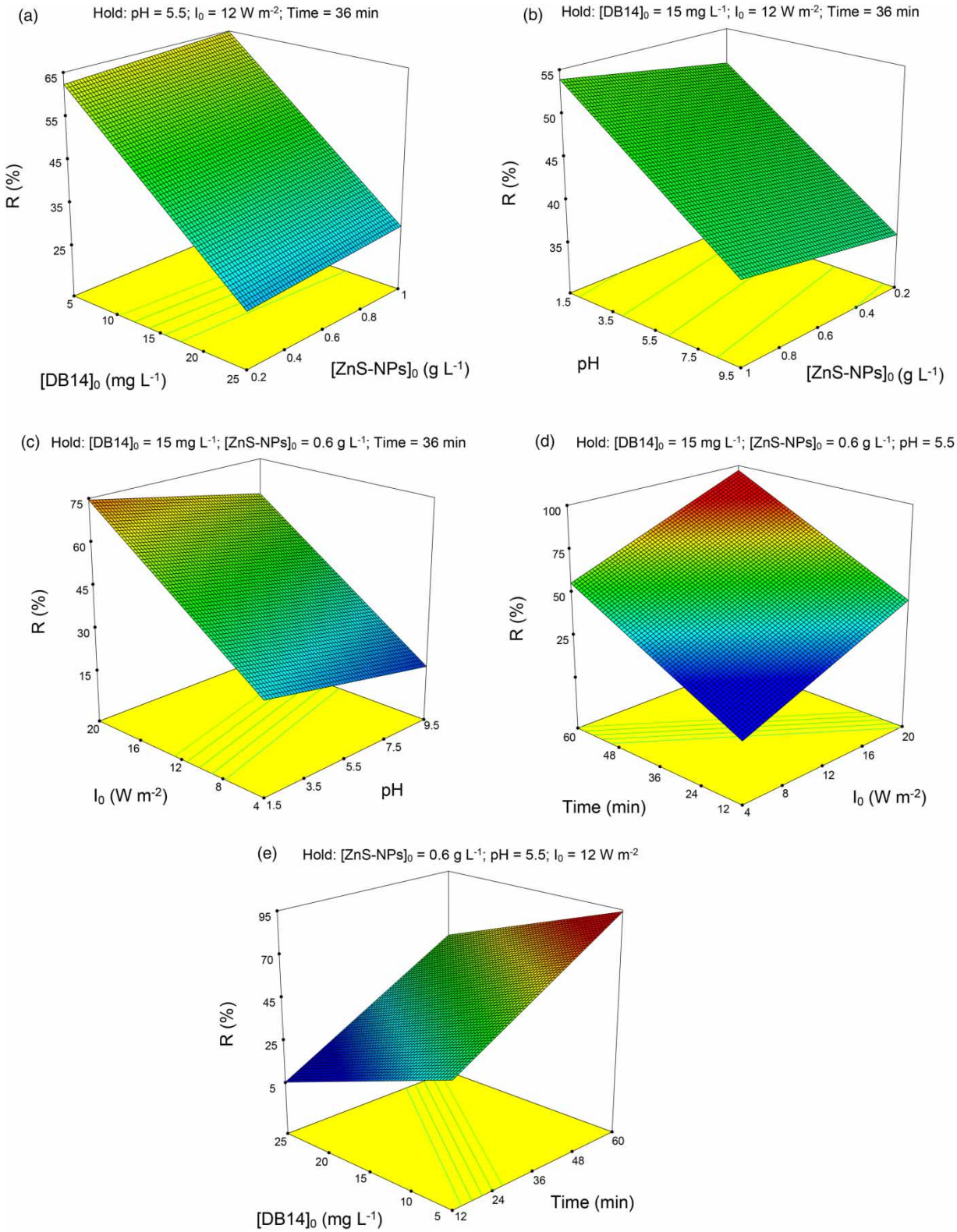

Figure 4 | Effect of operational variables on the DB14 removal by UV/ZnS-NPs process: (a) initial DB14 concentration and ZnS-NPs amount; (b) pH and ZnS-NPs amount; (c) pH and UV light intensity; (d) UV light intensity and irradiation time; (e) initial DB14 concentration and irradiation time.

Table 5 | Values of operational variables in kinetics study along with experimental and calculated k_{ap} values

	Operational parameters			k_{ap}	
Run	$[DB14]_0$ (mg L^{-1})	pH	I_0 (W m^{-2})	Experimental	Calculated
1	5	5.5	12	0.58	0.60
2	10	5.5	12	0.35	0.33
3	15	5.5	12	0.25	0.23
4	20	5.5	12	0.18	0.18
5	25	5.5	12	0.15	0.15
6	15	5.5	12	0.22	0.20
7	15	5.5	12	0.24	0.22
8	15	5.5	12	0.26	0.2
9	15	5.5	12	0.27	0.24
10	15	5.5	12	0.29	0.25
11	15	1.5	12	0.37	0.40
12	15	3.5	12	0.24	0.24
13	15	5.5	12	0.21	0.23
14	15	7.5	12	0.17	0.18
15	15	9.5	12	0.11	0.12
16	15	5.5	4	0.17	0.18
17	15	5.5	8	0.18	0.19
18	15	5.5	12	0.22	0.23
19	15	5.5	16	0.35	0.37
20	15	5.5	20	0.41	0.40

assumption proposed by Beltran-Heredia *et al.* (2001), $KC + \sum K_i C_i$ is equal to KC_0 (C_0 is the initial dye concentration) and under these circumstances:

$$r = -\frac{dC}{dt} = \frac{kKC}{1 + KC_0} \tag{12}$$

By considering the apparent rate constant, k_{ap} (i.e., $k_{app} = (kK)/(1 + KC_0)$), Equation (12) can be summarized as a pseudo-first-order kinetic model (Soltani & Entezari 2013):

$$r = -\frac{dC}{dt} = k_{app}C \rightarrow \ln\frac{C_0}{C_t} = k_{ap}t \tag{13}$$

Semi-logarithmic graphs of the DB14 concentration versus irradiation time at different values of operational variables (listed in Table 5) were drawn, and achievement of direct lines in all of the experiments (Figure 5) confirmed the fitting of this process by pseudo-first-order kinetics model. It is to be noted that results of RSM indicated photocatalyst dosage effect can be neglected, therefore this parameter was removed from kinetics study.

The non-linear relationship of k_{ap} with each of the operational variables is expressed by the following equation (Marandi *et al.* 2012):

$$k_{ap} = \alpha(\text{operational variables})^{\beta} \tag{14}$$

where α and β are the non-linear equation constants which are presented in Figure 6.

It is clear from Figure 6, k_{ap} increases with increment of UV light intensity, whereas k_{ap} decreases with increasing initial dye concentration and pH. These results are in good agreement with the interpretation of three-dimensional graphs (Figure 4) and thus, k_{ap} is a function of the operational variables as follows:

$$k_{ap} = k' \frac{I_0^a}{[DB14]_0^b \, pH^c} \tag{15}$$

where a, b, and c are the superscripts of the non-linear equations reported in Figure 6, and k' can be computed for each run by applying known values of k_{ap} and operational variables. The average value of k' was achieved as 2.85.

By substitution of the mean value of k' and relevant constants in Equation (15), the following equation as a kinetics model for anticipation of k_{ap} in various experimental conditions can be rewritten:

$$k_{ap} = 2.85 \frac{I_0^{0.5376}}{[DB14]_0^{0.85} \, pH^{0.85}} \tag{16}$$

By comparing the experimental and model predicted k_{ap} values (listed in Table 5), it can be seen that this model explains perfectly the results in the experimental range studied.

CONCLUSION

The results of the current study led to the conclusion that UV/ZnS-NPs process is an efficient method for removal of

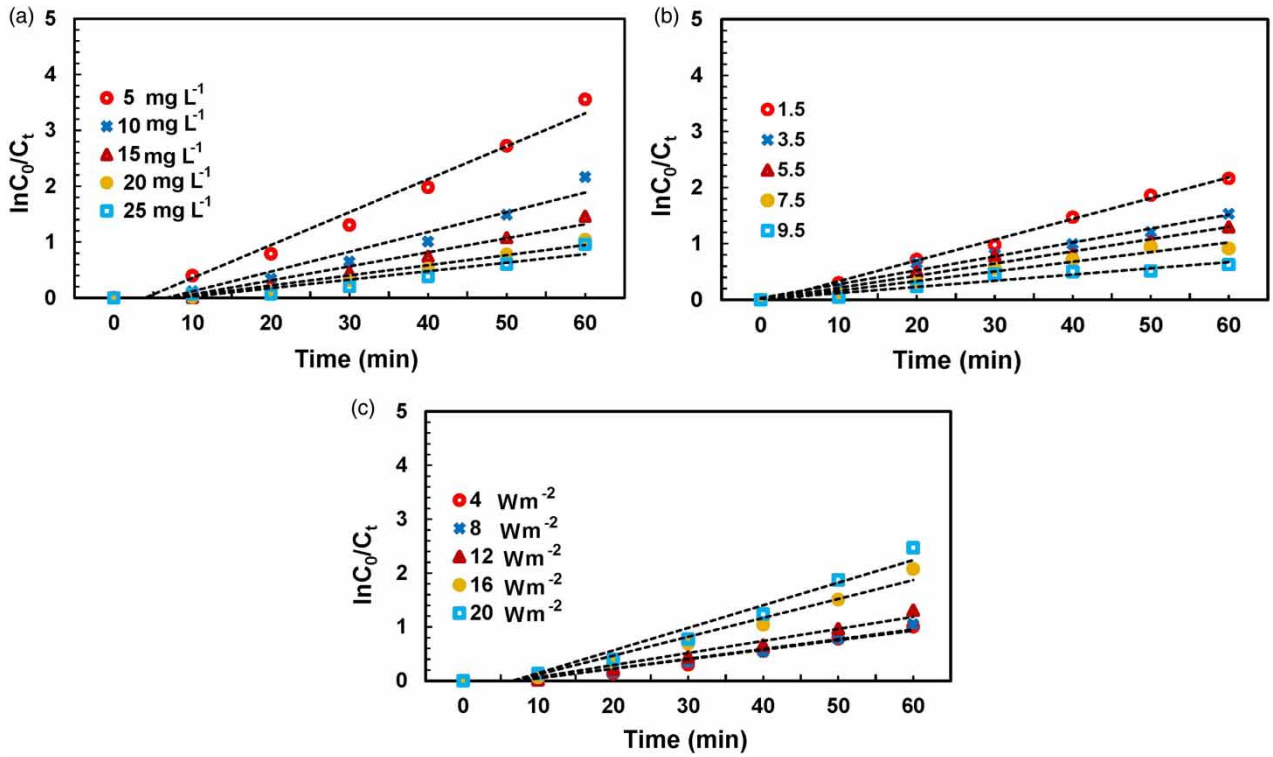

Figure 5 | Semi-logarithmic plots of the DB14 concentration versus irradiation time at different: (a) initial concentrations of DB14; (b) pHs; (c) irradiation intensities.

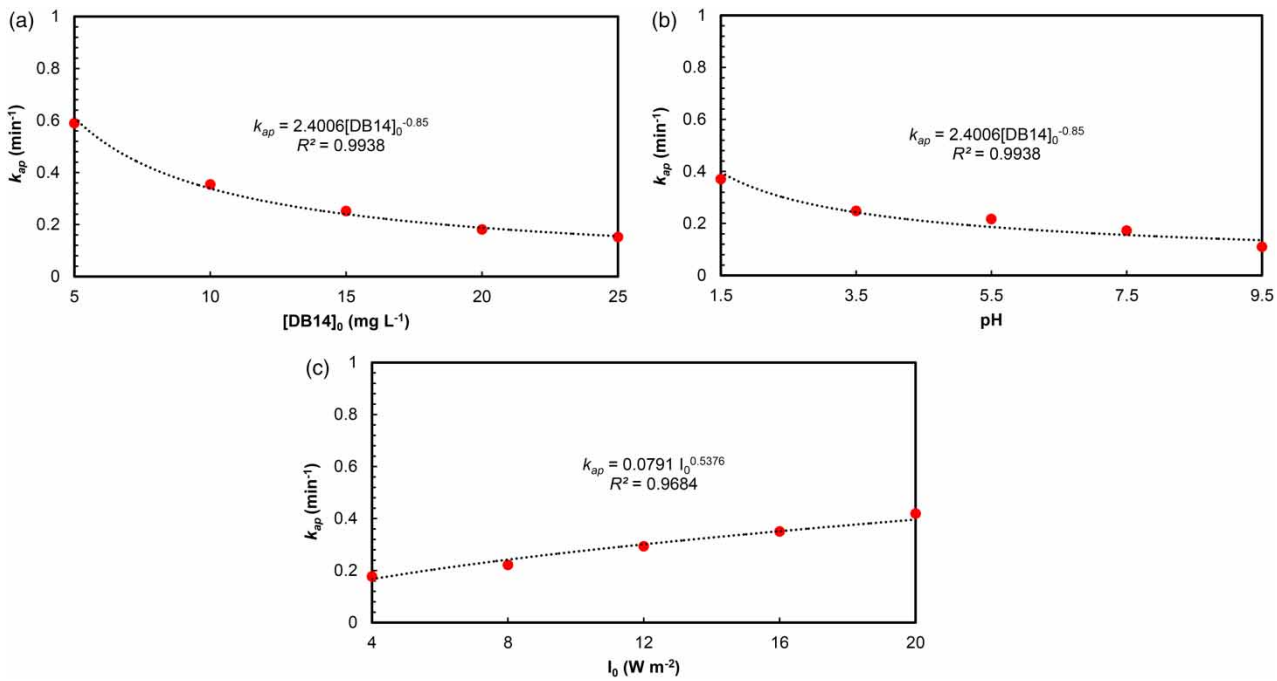

Figure 6 | The k_{ap} values affected by different levels of: (a) initial DB14 concentration; (b) pH; (c) UV light intensity.

DB14 dyestuff from the aquatic environment. RSM was employed for optimization of dye removal process and the findings demonstrated that the intensity and the duration of UV light irradiation were the most important variables in the photocatalytic removal of DB14. Under optimum conditions, dye removal efficiency reached 88.26%. Moreover, kinetic modeling was developed based on the non-linear regression analysis for the removal of DB14 dye using UV/ZnS-NPs system. It was found that the rate of dye removal followed the Langmuir–Hinshelwood pseudo-first-order kinetics model and an empirical mathematical equation was obtained for estimation of apparent pseudo-first-order rate constant (k_{ap}) as a function of the operational variables.

ACKNOWLEDGEMENT

The authors would like to thank the Tabriz Branch, Islamic Azad University for financial support.

REFERENCES

Agarwal, S., Tyagi, I., Gupta, V. K., Golbaz, F., Nozad Golikand, A. & Moradi, O. 2016 Synthesis and characteristics of polyaniline/zirconium oxide conductive nanocomposite for dye adsorption application. *Journal of Molecular Liquids* **218**, 494–498.

Antonin, V. S., Garcia-Segura, S., Santos, M. C. & Brillas, E. 2015 Degradation of Evans Blue diazo dye by electrochemical processes based on Fenton's reaction chemistry. *Journal of Electroanalytical Chemistry* **747** (15), 1–11.

Asfaram, A., Ghaedi, M., Yousefi, F. & Dastkhoon, M. 2016 Experimental design and modeling of ultrasound assisted simultaneous adsorption of cationic dyes onto ZnS: Mn -NPs-AC from binary mixture. *Ultrasonics Sonochemistry* **33**, 77–89.

Barragan, B. E., Costa, C. & Marquez, M. C. 2007 Biodegradation of azo dyes by bacteria inoculated on solid media. *Dyes and Pigments* **75**, 73–81.

Behnajady, M. A. & Modirshahla, N. 2006 Nonlinear regression analysis of kinetics of the photocatalytic decolorization of an azo dye in aqueous tio$_2$ slurry. *Photochemical & Photobiological Sciences* **5**, 1078–1081.

Behnajady, M. A., Mansoriieh, N., Modirshahla, N. & Shokri, M. 2012 Influence of operational parameters and kinetics analysis on the photocatalytic reduction of Cr(VI) by immobilized ZnO. *Environmental Technology* **33**, 265–271.

Beltran-Heredia, J., Torregrosa, J., Dominguez, J. R. & Peres, J. A. 2001 Oxidation of p-hydroxybenzoic acid by UV radiation and by Tio$_2$/UV radiation: comparison and modelling of reaction kinetic. *Journal of Hazardous Materials* **83** (3), 255–264.

Chandrakar, R. K., Baghel, R. N., Chandra, V. K. & Chandra, B. P. 2015 Synthesis, characterization and photoluminescence studies of undoped ZnS nanoparticles. *Superlattices and Microstructures* **84**, 132–143.

Di Paola, A., Garcia-Lopez, E., Marci, G. & Palmisano, L. 2012 A survey of photocatalytic materials for environmental remediation. *Journal of Hazardous Materials* **211–212**, 3–29.

Ertugay, N. & Nuran Acar, F. 2014 The degradation of Direct Blue 71 by sono, photo and sonophotocatalytic oxidation in the presence of ZnO nanocatalyst. *Applied Surface Science* **318**, 121–126.

Guinier, A. 1963 *X-ray Diffraction in Crystals, Imperfect Crystals, and Amorphous, X-ray Diffraction.* Freeman, San Francisco, CA.

Hassani, A., Khataee, A. R. & Karaca, S. 2015 Photocatalytic degradation of ciprofloxacin by synthesized tio$_2$ nanoparticles on montmorillonite: effect of operation parameters and artificial neural network modeling. *Journal of Molecular Catalysis A: Chemical* **409**, 149–161.

Kaur, J., Sharma, M. & Pandey, O. P. 2015 Structural and optical studies of undoped and copper doped zinc sulphide nanoparticles for photocatalytic application. *Superlattices and Microstructures* **77**, 35–53.

Khataee, A. R. & Zarei, M. 2011 Photocatalysis of a dye solution using immobilized ZnO nanoparticles combined with photoelectrochemical process. *Desalination* **273**, 453–460.

Khataee, A. R., Arefi-Oskoui, S., Fathinia, M., Fazli, A., Shahedi, A., Hanifehpour, Y. & Joo, W. J. 2015 Photocatalysis of sulfasalazine using Gd-doped PbSe nanoparticles under visible light irradiation: kinetics, intermediate identification and phyto-toxicological studies. *Journal of Industrial and Engineering Chemistry* **30**, 134–146.

Kong, W., Qu, H., Chen, P., Ma, W. & Xie, H. 2016 Property of Cu_2O-CuO/ZSM-5 nanocomposite and degradation process of azo dye AO7 without sacrificial agent (H_2O_2). *Water Science and Technology* **73** (11), 2747–2753.

Lalnunhlimi, S. & Krishnaswamy, V. 2016 Decolorization of azo dyes (Direct Blue 151 and Direct Red 31) by moderately alkaliphilic bacterial consortium. *Brazilian Journal of Microbiology* **47** (1), 39–46.

Lelario, F., Brienza, M., Bufo, S. A. & Scrano, L. 2016 Effectiveness of different advanced oxidation processes (AOPs) on the abatement of the model compound mepanipyrim in water. *Journal of Photochemistry and Photobiology A: Chemistry* **321**, 187–201.

Marandi, R., Olya, M. E., Vahid, B., Khosravi, M. & Hatami, M. 2012 Kinetic modeling of photocatalytic degradation of an azo dye using nano-TiO_2/Polyester. *Environmental Engineering Science* **29** (10), 957–963.

Padmanaban, V. C., Giri Nandagopal, M. S., Achary, A., Vasudevan, V. N. & Selvaraju, N. 2016 Optimisation of radiolysis of Reactive Red 120 dye in aqueous solution using ionising ^{60}CO gamma radiation by response surface

methodology. *Water Science and Technology* **73** (12), 3041–3048.

Pouretedal, H. R., Norozi, A., Keshavarz, M. H. & Semnani, A. 2009 Nanoparticles of zinc sulfide doped with manganese, nickel and copper as nanophotocatalyst in the degradation of organic dyes. *Journal of Hazardous Materials* **162**, 674–681.

Punzi, M., Anbalagan, A., Aragao Borner, S., Svensson, B. M., Jonstrup, M. & Mattiasson, B. 2015 Degradation of a textile azo dye using biological treatment followed by photo-Fenton oxidation: evaluation of toxicity and microbial community structure. *Chemical Engineering Journal* **270** (15), 290–299.

Saien, J., Ojaghloo, Z., Soleymani, A. R. & Rasoulifard, M. H. 2011 Homogeneous and heterogeneous AOPs for rapid degradation of Triton X-100 in aqueous media via UV light, nano titania hydrogen peroxide and potassium persulfate. *Chemical Engineering Journal* **167** (1), 172–182.

Sakkas, V. A., Azharul Islam, M., Stalikas, C. & Albanis, T. A. 2010 Photocatalytic degradation using design of experiments: a review and example of the Congo red degradation. *Journal of Hazardous Materials* **175** (1–3), 33–44.

Sheidaei, B. & Behnajady, M. A. 2015 Mathematical kinetic modelling and representing design equation for a packed photoreactor with immobilised TiO_2-P25 nanoparticles on glass beads in the removal of C.I. Acid Orange 7. *Chemical and Process Engineering* **36**, 125–133.

Soltani, T. & Entezari, M. H. 2013 Photolysis and photocatalysis of methylene blue by ferrite bismuth nanoparticles under sunlight irradiation. *Journal of Molecular Catalysis A: Chemical* **377**, 197–203.

Wang, H. D., Yang, Q., Niu, C. H. & Badea, I. 2012 Adsorption of azo dye onto nanodiamond surface. *Diamond and Related Materials* **26**, 1–6.

Yatmaz, H. C., Akyol, A. & Bayramoglu, M. 2004 Kinetics of the photocatalytic decolorization of an azo reactive dye in aqueous ZnO suspensions. *Industrial & Engineering Chemistry Research* **43**, 6035–6039.

Yin, L., Zhang, D., Wang, D., Kong, X., Huang, J., Wang, F. & Wu, Y. 2016 Size dependent photocatalytic activity of ZnS nanostructures prepared by a facile precipitation method. *Materials Science and Engineering B* **208**, 15–21.

Zhang, Y., Gao, F., Wanjala, B., Li, Z., Gernigliaro, G. & Gu, Z. 2016 High efficiency reductive degradation of a wide range of azo dyes by SiO_2-Co core-shell nanoparticles. *Applied Catalysis B: Environmental* **199**, 504–513.

First received 20 October 2016; accepted in revised form 16 August 2017. Available online 9 October 2017